Three Types of Adsorptions of Nitric Oxide on the MgO Surface

Yasunori Yanagisawa,* Kei Kuramoto, and Shin-ichi Yamabe

Department of Materials Science, Nara University of Education, Takabatake-cho, Nara 630-8528, Japan

Received: May 5, 1999; In Final Form: September 13, 1999

FT-IR spectroscopic studies of the adsorption of natural and ^{18}O-enriched NO gases on thermally and cleaned MgO powders were carried out. The temperature dependence of the IR spectra was investigated to characterize the adsorbate species. Three types [1, 2, and 3] of NO adsorptions were obtained in the wavenumber region of 1500−1000 cm^{-1}. Those types were examined using density functional theory [(U)B3-LYP/6-31G*] vibrational analyses of $(MgO)_n$−NO cluster calculations. Types 1, 2, and 3 were assigned to monodentate, asymmetric, and symmetric bidentate geometries, respectively. A type 4, a "tridentate" model which involves a NO_3-like species, was calculated and was found to give wavenumbers of less than 1000 cm^{-1}. The splitting of IR bands of type 3 due to the $^{15}N^{18}O$ adsorbate was ascribed to the oxygen exchange, $^{15}N^{18}O \rightarrow {}^{15}N^{16}O$, via the reaction $^{16}O-{}^{15}N-{}^{18}O \rightarrow {}^{16}O-{}^{15}N-{}^{16}O$ on MgO surfaces.

I. Introduction

The interactions of nitric oxide with metal oxides have been widely investigated for their ability to eliminate atmospheric pollutants from waste gases. The adsorption of NO on metal oxides leads to the catalytic decomposition of NO to N_2 and O_2 and/or the formation of N_2O.[1,2] Surface sites, such as coordinatively unsaturated cations and anions (M_{CUS}'s and O_{CUS}'s, respectively) at steps and kinks, play an important role in the catalytic processes.

By using IR measurements, a variety of surface complexes, such as NO^-, NO_2^- with various configurations, and $(NO)_2^-$ species, have been identified after a huge amount of NO adsorption on MgO powders and adsorption/desorption processes were suggested.[3] However, the atomistic structures of adsorbates including adsorption sites were not determined precisely. More recently, we have described oxygen isotope exchange between $N^{18}O$ and MgO powders using temperature-programmed desorption (TPD) measurements, and the exchange process was tentatively explained by NO_2-type adsorbates and subsequent surface migrations.[4]

The determination of vibrational frequencies by ab initio calculations is becoming increasingly important. Theoretically obtained frequencies can be used to predict and assign experimental IR and Raman frequencies.[5] While theoretical frequencies do not contain the anharmonicity, scaling factors which involve it have been developed and established.[6] In view of the accuracy of recent theoretical frequencies, ab initio calculations are expected to identify the adsorbate species on the surface. In particular, the radical species $NO^\bullet$ would be bound to the MgO surface via a covalent bond.

In the present study, an IR-theory combined analysis was made in order to characterize the NO adsorption patterns on an MgO surface, while IR measurements of the adsorbed species and a test for the isotope effect were performed for comparison with the theoretical frequencies. Such a systematic analysis has not been reported so far to our knowledge. It will be shown that the NO radical is linked with the surface oxygen atoms in three ways to give specific adsorbed structures. In this work, we report the FT-IR spectroscopic investigations of the adsorption of ^{18}O-enriched NO on MgO powders in relation to TPD results. A vibrational analysis of density functional theory (DFT) calculations was carried out for various plausible adsorbed species at Mg_{CUS} and O_{CUS} surface ions. Computed harmonic frequencies are compared with observed ones. Since the $NO^\bullet$ radical is a reactive species, it will be bound to a specific lattice oxygen. That is, the NO adsorption would be a local reaction on the surface. Cluster-model calculations seem to be meaningful to describe such a chemical problem.

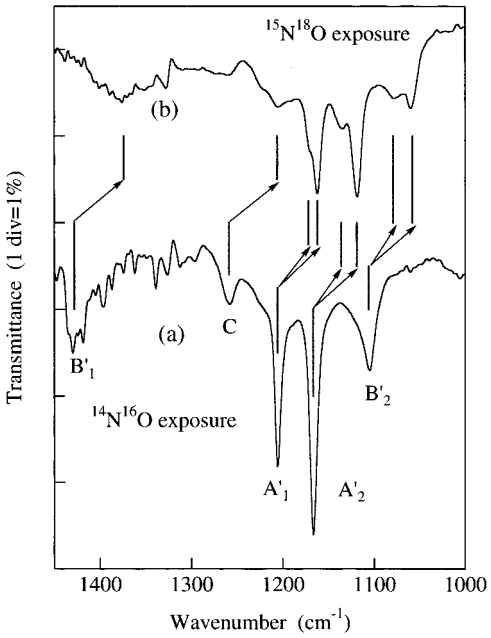

Figure 1. IR spectra of MgO powders at room temperature after (a) $^{14}N^{16}O$ and (b) $^{15}N^{18}O$ exposures of 2.0×10^{-3} Torr for 2 min following evacuation. Wavenumbers of peaks are given in Scheme 1.

II. Experimental and Computational Section

Pressed disks of MgO powder ("Specpure" grade from Johnson-Matthey Chem. Ltd.) were preheated at 1023 K for several hours in a quartz cell before each run under pressure of $\sim 10^{-8}$ Torr. IR spectra were measured with ca. 0.05 g sample

10.1021/jp991478w CCC: $18.00
Published on Web 11/23/1999

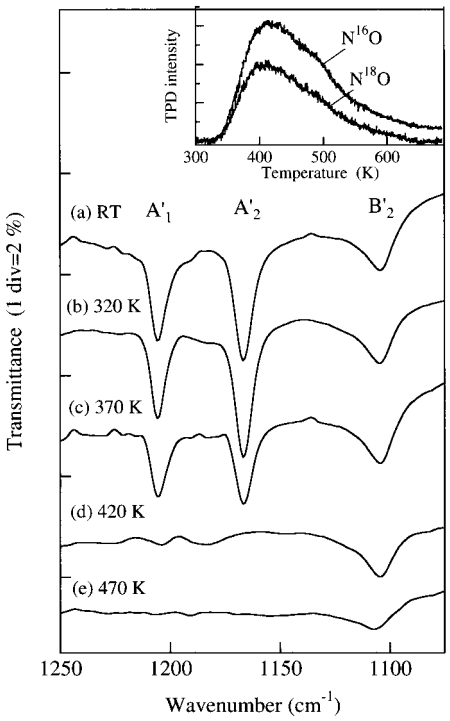

Figure 2. Measured IR spectra of $N^{16}O$ adsorption on MgO at room temperature after exposure of 2.0×10^{-3} Torr for 2 min following evacuation (a), and heating to 320 (b), 370 (c), 420 (d), and 470 K (e) at a heating rate of 0.25 K/s. Relatively strong and sharp bands of groups A′ and B′ are shown. TPD profiles of $N^{16}O$ and $N^{18}O$ gases after $N^{18}O$ exposure (8.0×10^{-6} Torr for 3 min) at RT from MgO powders are shown in the inset.[4]

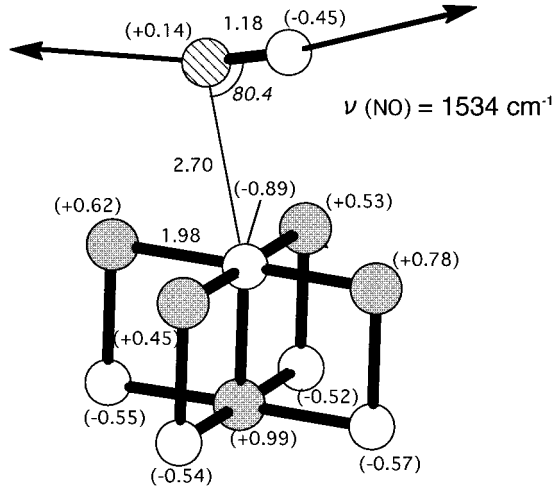

Figure 3. An $(MgO)_5NO$ geometry optimized with UB3-LYP/6-31G*. Empty, black, and shaded circles stand for oxygen, magnesium, and nitrogen atoms, respectively. Among $3N - 6$ vibrational modes, the N−O stretching mode is depicted. The corresponding scaled frequency (ν) is also shown. The experimental Mg−O distance is 2.1065 Å. Distances are in angstroms, and angles are in degrees.

disks in a quartz cell with CaF_2 windows in the wavenumber region of 2500−1000 cm^{-1} by using an FT-IR spectrometer (Perkin-Elmer, System 2000). After baking, no traces of hydroxyl and carbonate groups were detected. The sample was exposed to $^{14}N^{16}O$ (99.5% purity, Takachiho Kagaku Ltd.) and $^{15}N^{18}O$ (99.8% ^{15}N and 97.5% ^{18}O isotopic purity, Isotech Inc.) gases at RT through a variable-leak valve without any purification. During NO exposure, the cell was kept at a constant pressure in the range 0.001−0.1 Torr by monitoring it with a Pirani gauge. Spectra were recorded in a transmission mode

SCHEME 1: Summary and Tentative Assignment of the Observed IR Frequencies[a]

Suggested types	Structural models	Wavenumbers(cm^{-1}) (a) Natural $^{14}N^{16}O$		(b) Isotope $^{15}N^{18}O$	
bidentate NO_2^- (Group A')	Mg O N O	A_1'	1205 (1208)	A_{1a}'	1171
				A_{1b}'	1162
		A_2'	1167 (1168)	A_{2a}'	1134
				A_{2b}'	1118
			--- (850)		---
monodentate NO_2^- (Group B')	Mg O N O	B_1'	1430 (1404)		1375
		B_2'	1104 (1120)	B_{2a}'	1079
				B_{2b}'	1058
		--- (850)		---	
NO^- (Group C)	Mg N O	1257 (1160)		1203	

[a] Values in parentheses are those in ref 3. Columns a and b correspond to (a) and (b) in Figure 1, respectively.

SCHEME 2: Four Types of the NO• Absorption on the MgO Surface for ab Initio Calculations

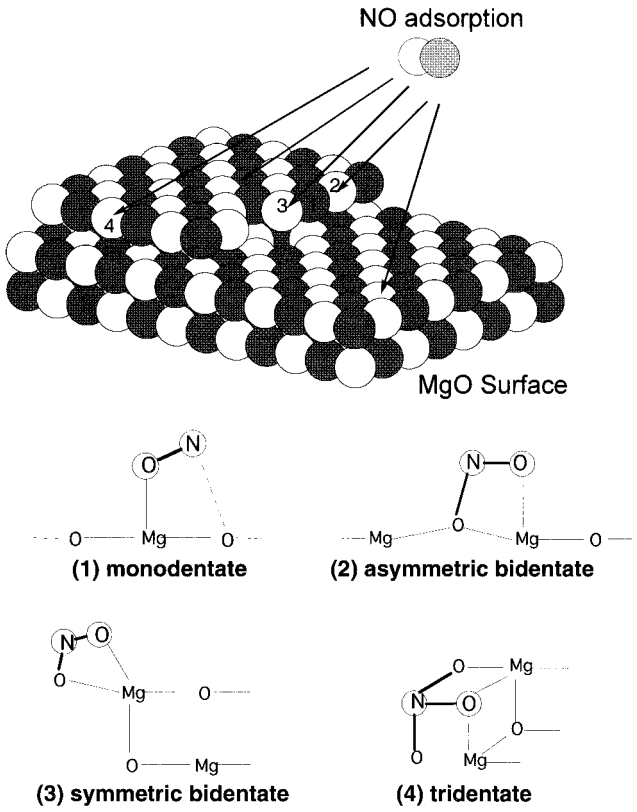

with 64 scans and 4 cm^{-1} resolution. All spectra were depicted as differences of samples with and without adsorbed species.

DFT calculations were performed using the GAUSSIAN 94[7] program on the CONVEX SPP 1200/XA computer at the Information Processing Center of Nara University of Education. All the geometries were optimized using the (U or R) Becke3lyp/6-31G* method[8] which is known to be state-of-the art in regard to its accuracy and practicality.[9] Subsequently, B3-LYP/6-31G*

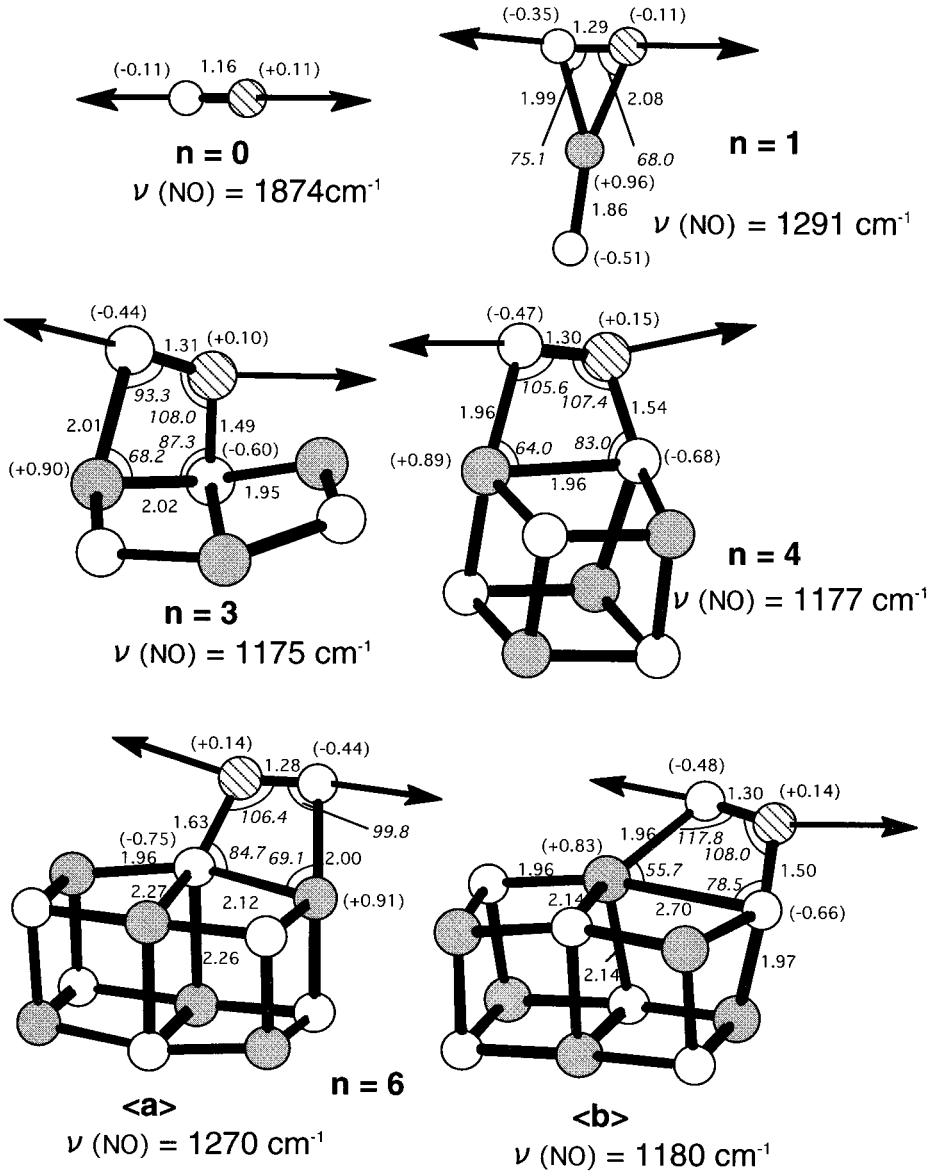

Figure 4. Geometries of $(MgO)_nNO^•$ clusters, N−O stretching modes, and the corresponding wavenumbers.

SCHEME 3: A Geometric Difference by an Electron

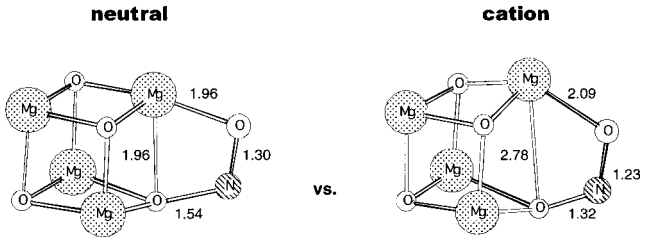

SCHEME 4: Oxygen Exchange via the Type 3 Adsorption on the MgO Surface

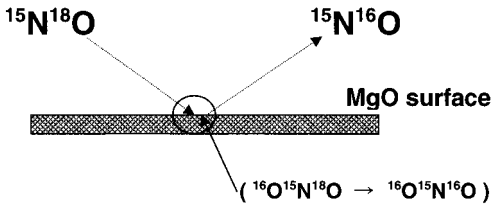

vibrational analyses were carried out to evaluate harmonic frequencies and IR intensities. Those frequencies are scaled down by 0.941 to consider the anharmonicity. The scale factor was determined by comparison of calculated wavenumbers of $NO^•$ and $NO_2^•$ radicals with experimental ones. For some anionic species related to this work, B3-LYP/6-31+G* geometry optimizations and vibrational analyses were made to assess the B3-LYP/6-31G* data. Usually, anionic and radical systems are described properly by inclusion of the diffuse orbitals.[10] But, the present cluster size is too large for us to use the 6-31+G* basis set. The assessment of small anionic clusters showed that B3-LYP/6-31G* wavenumbers may be applicable to the present assignment (see ref 13). The convergence criterion on the first derivative of the total energy is 0.0003 hartree/bohr (default value).

III. Experimental Results and Discussion

Figure 1a shows IR spectra measured after $N^{16}O$ exposure (2.0×10^{-3} Torr, 2 min) to MgO powders at RT followed by evacuation. The absorption bands of part a were observed at 1430, 1257, 1205, 1167, and 1104 cm^{-1}. No bands were

SCHEME 5: Four Types of the NO Absorption on the MgO Surface

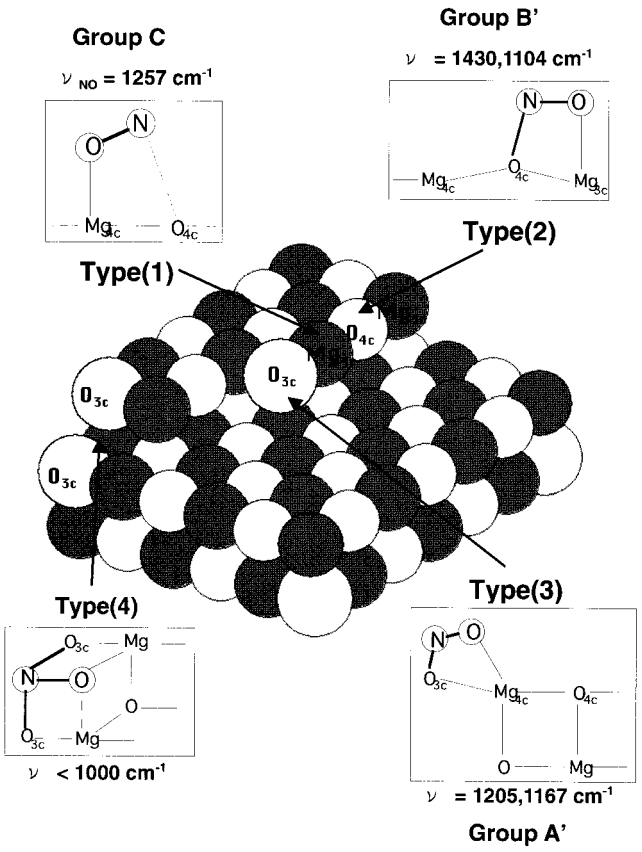

observed above 1500 cm^{-1}. The bands were almost similar to those observed after NO admission at low pressures (~0.03 Torr) on MgO powders reported by Cerruti et al.[3] The group of bands at 1205 and 1167 cm^{-1} corresponds to the species A′ (1208, 1168, and 850 cm^{-1}),[3] which was assumed to be an NO_2^- ion on the surfaces. The 850 cm^{-1} band was not observed here because of the absorption of CaF_2 windows. The group of bands at 1430 and 1104 cm^{-1} corresponds to the species B′ (1404 and 1120 cm^{-1})[3] and was assumed to be an ONO^- species. Hereafter, IR bands of species A′ and B′ are denoted as follows: 1205 (A'_1), 1167 (A'_2), 1430 (B'_1), and 1104 cm^{-1} (B'_2), respectively. The weak band at 1257 cm^{-1} is labeled as a species C. The character of the species is uncertain at the present stage and will be examined theoretically. The IR bands corresponding to $(NO)_2^{2-}$ species (1384, 1190, 1150, and 830 cm^{-1})[3] were not observed because NO admission was carried out under low pressures.

Figure 1b shows the IR spectrum measured after $^{15}N^{18}O$ exposure (2.0×10^{-3} Torr, 2 min) at RT followed by evacuation. The IR bands of species A′ and B′ are observed at RT and shift to lower frequencies due to the isotope effect of both ^{15}N and ^{18}O. Especially, the 1206 (A'_1), 1167 (A'_2), and 1104 cm^{-1} (B'_2) bands split into two bands at 1171 (A'_{1a}, shoulder) and 1162 cm^{-1} (A'_{1b}), 1134 (A'_{2a}) and 1118 (A'_{2b}) cm^{-1}, and, 1079 (B'_{2a}) and 1058 cm^{-1} (B'_{2b}), respectively, while the splitting for the bands of species B'_1 is not clear. The band of species C seems to shift to lower frequency from 1257 to 1203 cm^{-1}, while the splitting is not clear because of the signal weakness. Thus, it is reasonable to assume that the species A′ and B′ contain two O atoms (i.e., zero and one ^{18}O atom, indicating $N^{16}O_2$ and $N^{16}O^{18}O$ forms) and oxidation of NO may occur including an O_{CUS} atom on the surfaces. The adsorbed $N^{18}O$ has already undergone an isotope exchange with an O_{CUS}

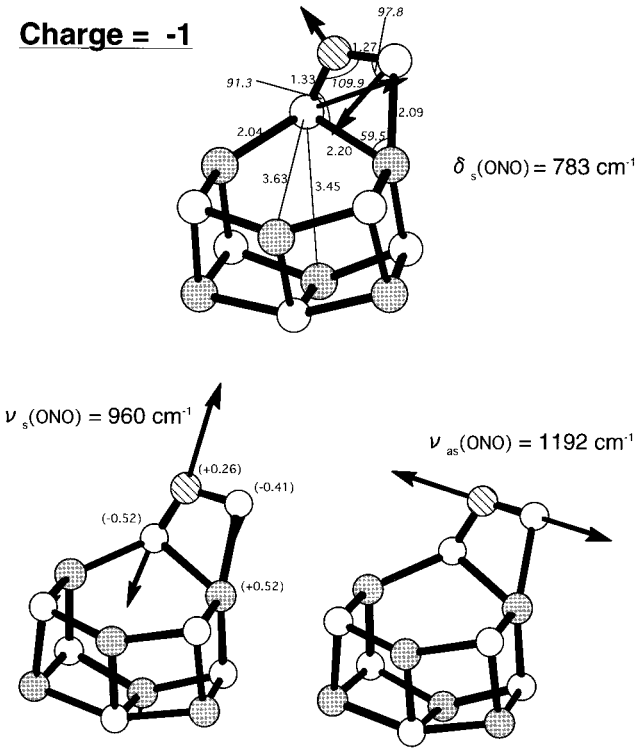

Figure 5. Geometry of $(MgO)_6NO^-$ and three specific vibrations.

to a considerable amount through NO_2-type intermediates. The $N^{16}O_2$ species is formed in addition to an $N^{16}O^{18}O$ species after the exposure at RT.

Figure 2 shows IR spectra measured after $N^{16}O$ exposure at RT followed by evacuation at successively higher temperatures up to 470 K. The species A′ completely disappears by heat increase up to 420 K (spectra a−d). The species B′ does not disappear completely up to 470 K (spectra a−e). The weak band at 1257 cm^{-1} (species C) has disappeared below 470 K, suggesting that this species is different from species A′ and B′. The main TPD profiles of $N^{16}O$ and $N^{18}O$ gases after $N^{18}O$ exposure (8.0×10^{-6} Torr for 3 min) at RT are shown in the insert of Figure 2.[4] Thermal desorptions (TDs) of $N^{16}O$ and $N^{18}O$ are observed in the temperature region of 350−500 K, while no TD of O_2 was observed. This fact suggests that the adsorbed NO may not dissociate to form N_2 and O_2 species. Those TDs of $N^{16}O$ and $N^{18}O$ occur at the same temperature region as that of the disappearance of the IR bands of species A′ (and partly species B′). The coincidence indicates that the NO TPD is mainly originated from the NO_2 type adsorbates on the surface.

The present IR results are summarized in Scheme 1. In the next section, this tentative assignment will be revised on the basis of computational results.

IV. Results of Calculations and Discussions

DFT calculations of cluster models, $(MgO)_n\cdots NO^\bullet$ ($n = 0$, 1, 2, . . . 6) and their charged ones (cation and anion closed-shell species) were performed. The stretching frequency of the free radical, NO, is calculated to be 1875 cm^{-1}, which is in good agreement with the observed one, 1858 cm^{-1}.[11] The diatomic radical may be bound to the surface, resulting in $NO_2^\bullet$ or NO_2^- species. Three computed frequencies of the $NO_2^\bullet$ radical are 705 (750), 1322 (1320), and 1618 (1621) cm^{-1}, respectively, where values in parentheses are experimental ones.[11] The calculated frequencies of the NO_2^- anion are 745,

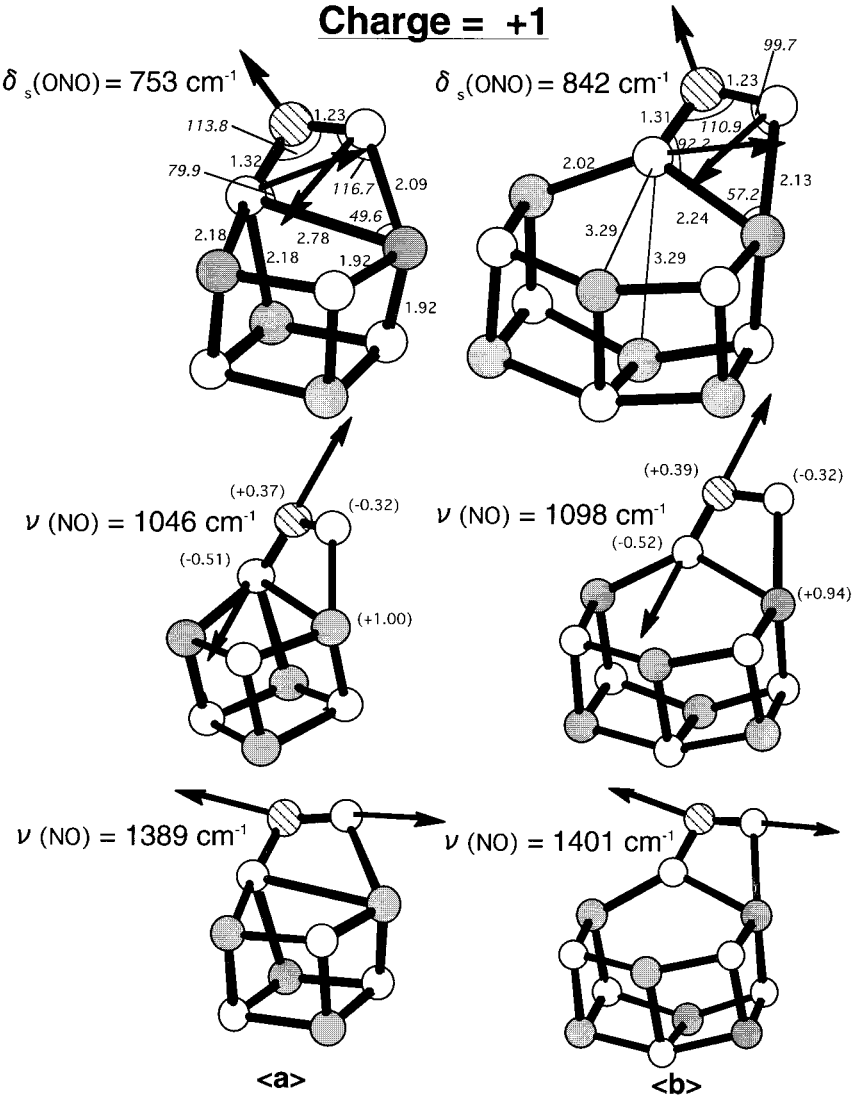

Figure 6. $(MgO)_4NO^+$ (*a*) and $(MgO)_6NO^+$ (*b*) geometries and their specific vibrations.

1262, and 1297 cm^{-1}. In the previous section, IR-observed frequencies have been shown to be 850−1430 cm^{-1}. Since the MgO ionic crystal has frequencies, 202−690 cm^{-1} (calculated by $(MgO)_6$ clusters), the frequencies obtained in this IR measurement would come from the NO_2-like species on the MgO surface.

First, the NO• adsorption model on an MgO (001) flat surface, $(MgO)_5NO^•$ was examined. The optimized geometry and a stretching vibrational mode is shown in Figure 3. The NO• radical is linked with the central surface oxygen very weakly with the adsorption energy 0.52 eV. This physisorption gives a theoretical frequency of 1534 cm^{-1}, which is appreciably smaller than that of the free NO• radical, 1875 cm^{-1} (calculated). That wavenumber was not observed in the present IR measurement. Therefore, other sites on the surfaces should be investigated to specify the observed IR data. The Mulliken charges in parentheses (Figure 3) indicate that the NO radical is a charge acceptor in the NO···$(MgO)_5$ cluster.

Four models of NO• adsorption are considered and shown in Scheme 2. The optimized geometries of $(MgO)_n$···NO• ($n = 0$, 1, 3, 4, and 6) are shown in Figure 4. The NO stretching mode and the corresponding calculated wavenumber are sketched in respective geometries. In those geometries, the N···O bond is formed even in the Mg−ON monodentate model. Ledge ions on step and corner sites are targets for the NO adsorption at the $n \geq 3$ cluster. In Scheme 1, a wavenumber of 1257 cm^{-1} ("uncertain" species C) has been found in the present measurement. The number is assignable to 1270 cm^{-1} (calculated) of the $(MgO)_6NO$(a*)* model. In this model, a four-membered moiety is formed. Since two N−O distances are significantly different (1.28 and 1.63 Å), the model is not bidentate. If the $(MgO)_8NO$(a*)* model were adopted, the calculated value 1290 cm^{-1} would be shifted to a lower frequency through the stronger Mg···O attraction and the agreement between the IR observed frequencies and calculated frequencies would be closer. Thus, the experimental number 1257 cm^{-1} may be assigned to the monodentate adsorbate species (C) in Scheme 1 with the adjacent N···O attraction (1.63 Å) on the Mg_{CUS} at the step site.

In Scheme 2, a closer contact of the NO• radical with the MgO surface than the (1) monodentate has been shown as type 2. Various "asymmetric bidentate" geometries of $(MgO)_n$NO• have been sought. In the previous section, two IR-observed wavenumbers (species B′), 1430 and 1104 (and 850) cm^{-1}, have been assigned to one group. They would be related to some asymmetric bidentate model. However, no $(MgO)_n$NO model can reproduce the group of three wavenumbers, i.e., the asymmetric bidentate model. The neutral cluster model $(MgO)_n$-NO's failure to reproduce the wavenumbers of species B′ leads us to examine charged cluster models. Adsorptions of anionic

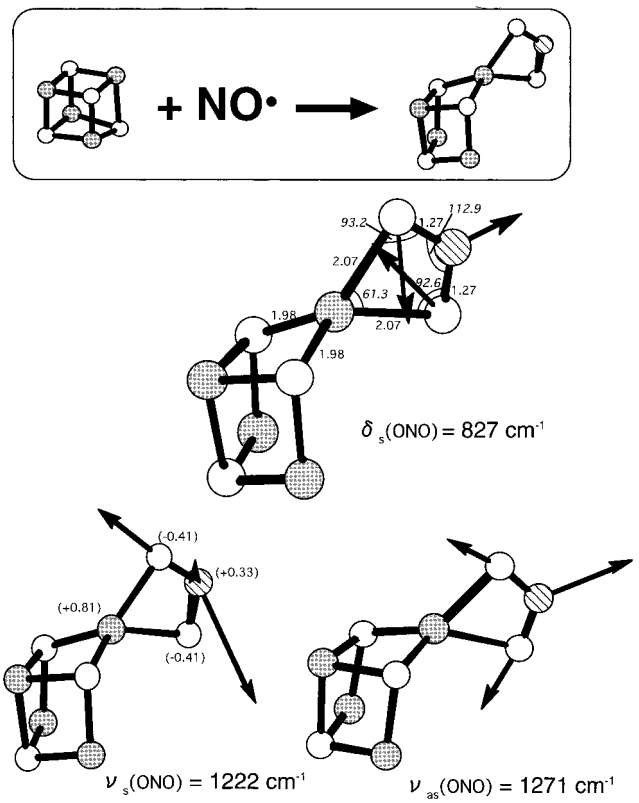

Figure 7. Deformed $(MgO)_4NO$ geometry and its three vibrations.

NO and N_2O_2 species on the CaO surface have been investigated theoretically.[12] For example, an oxygen vacancy (V_O^{2+}) would afford a cationic cluster system.

Figure 5 shows the optimized geometry of $(MgO)_6NO^{1-}$, which is a negatively charged system of $(MgO)_6NO$(a*)* shown in Figure 4. Through one-electron addition, the monodentate model is transformed to the asymmetric bidentate one. The $(MgO)_6NO^{1-}$ model gives three computed wavenumbers, 1192, 960 and 783 cm^{-1}. Three values are still somewhat different from the IR ones of species B′, 1430, 1104, (and 850) cm^{-1}. The former values correspond to the calculated values 1297, 1262, and 745 cm^{-1} of the free NO_2^- ion. A more asymmetric shape of the NO_2 moiety is required to reproduce, particularly, the observed 1430 cm^{-1}. Next, a positively charged cluster model $(MgO)_6NO^+$ is tested in Figure 6. A model $(MgO)_4NO^+$ is also examined in the figure to extract the key moiety. Deformation of the $(MgO)_6$ cluster in $(MgO)_6NO^+$ is interestingly similar to that in $(MgO)_6NO^-$. The NO_2Mg fragment of the cation cluster is slightly less symmetric (deviated from the C_{2v} symmetry) than that of the anion one. That slightly asymmetric geometry in $(MgO)_6NO^+$ gives three computed wavenumbers, 1401, 1098, and 842 cm^{-1}. Similarly, $(MgO)_4NO^+$ gives 1389, 1046, and 753 cm^{-1}. Both sets of three computed values are in good agreement with the IR observed set, species B′ (1430, 1104, and 850 cm^{-1}), in Scheme 1. Thus, the species B′ can be ascribed to the asymmetric bidentate model (type 2 in Scheme 2) of the positively charged cluster. An electron loss of the $(MgO)_4NO$ cluster induces a change in the geometry (Scheme 3) and accordingly three wavenumbers of the NO_2 moiety. The Mulliken electronic charges show that the terminal magnesium becomes cationic considerably in $(MgO)_4NO^+$ and $(MgO)_6NO^+$.

In Scheme 2, a symmetric (C_{2v}) bidentate model (3) has been suggested. This model would be related to the third group of IR data (species A′: 1205 and 1167 cm^{-1}, experimental data

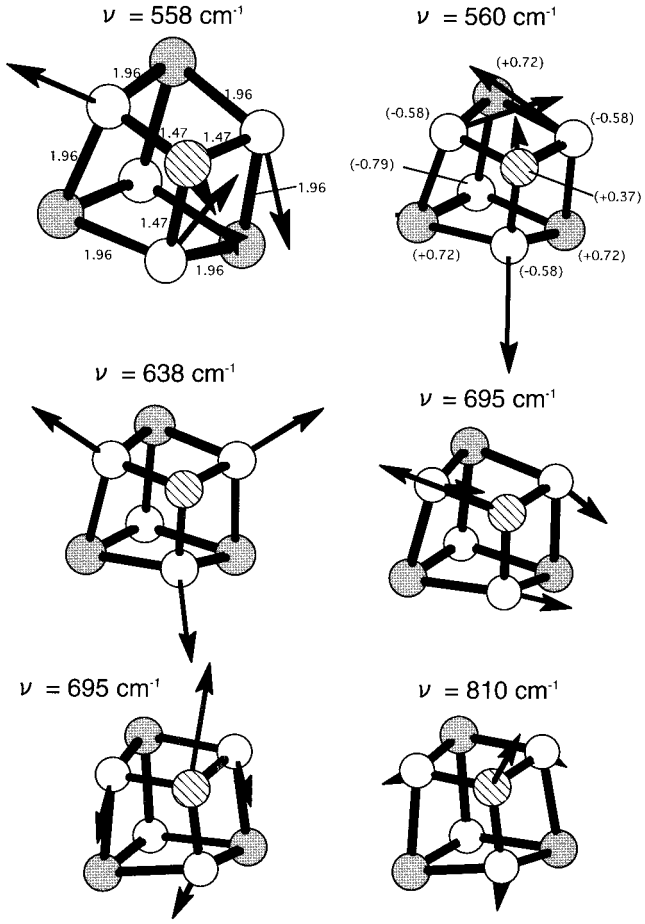

Figure 8. Geometry of $(MgO)_3NO$ and its six vibrations.

Vibration mode	Symmetric streching vibration	Antisymmetric streching vibration	Deformation vibration
^{16}O-^{14}N-^{16}O	1259 cm^{-1} (1271)	1219 cm^{-1} (1222)	824 cm^{-1} (827)
^{16}O-^{15}N-^{18}O	1224 cm^{-1} (1237)	1176 cm^{-1} (1177)	800 cm^{-1} (803)
^{16}O-^{15}N-^{16}O	1236 cm^{-1} (1249)	1193 cm^{-1} (1196)	819 cm^{-1} (823)

Figure 9. Calculated isotope effect on three wavenumbers in a model MgO_2N radical species (in the C_{2v} point group) and $(MgO)_4NO$ seen in Figure 7. Values without parentheses are wavenumbers of the MgO_2N model, and those with parentheses are of the $(MgO)_4NO$ geometry.

in Scheme 1). This prediction is based on a preliminary calculation of a four-atom radical species, MgO_2N of the C_{2v} symmetry, which gives the computed values 1259, 1219, and 824 cm^{-1}. Various $(MgO)_6NO^•$ geometries have been sought to describe the C_{2v} model. But this symmetric moiety cannot be obtained in the $(MgO)_6NO^•$ cluster. Next, $(MgO)_4NO$ geometries have been examined and a C_{2v}-symmetric moiety

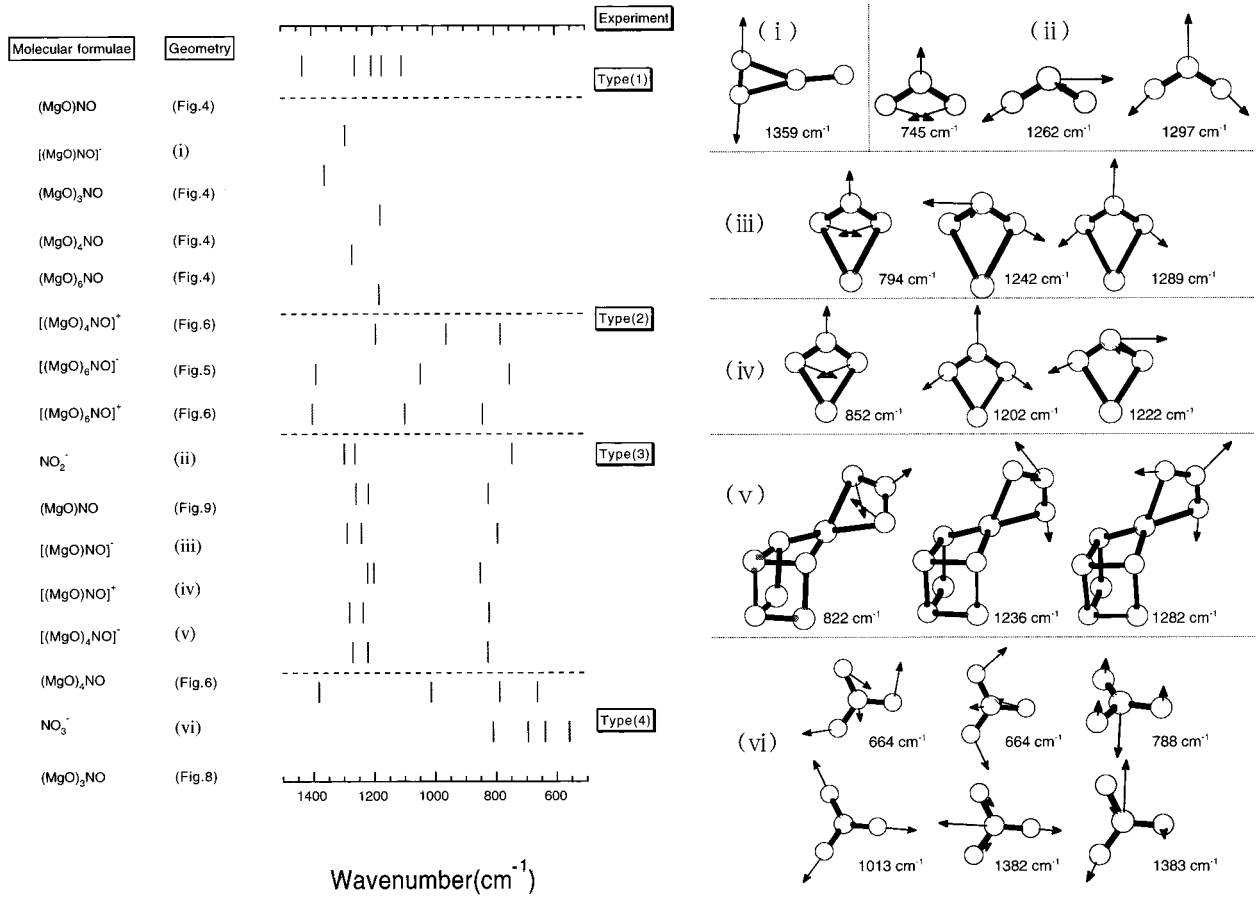

Figure 10. Wavenumbers obtained by cluster models including those in Figures 4−9. The present experimental data are also shown.

has been successfully obtained and is shown in Figure 7. This geometry has been optimized, starting from that of the cubic $(MgO)_4$ cluster plus the NO• radical. Three calculated wavenumbers are 1271, 1222, and 827 cm^{-1}. Although the former two are somewhat larger than the IR data, 1205 and 1167 cm^{-1} (species A′), their differences (1271−1222, calculated ≅ 1205−1167, experimental) are similar. The slight overestimate would come from the simplified model, $(MgO)_4NO$. The active NO• radical may bring about such a specific C_{2v}-symmetric moiety on the MgO surface. By nature, Coulombic attractions in Mg−O ionic bonds are of spherical potential and nondirectional. On the other hand, covalent bonds involving the NO species require the rigid directionality. When those bonds compete with each other on the surface, the MgO cluster is deformed so as to conform to the rigid directionality.

Finally, a "tridentate" model (4) in Scheme 2 is examined. The model involves a NO_3 type species and can be obtained in the kink site. Figure 8 shows that the NO• radical is bound to the site composed of $(MgO)_3$. The resultant $(MgO)_3NO$ is of the C_{3v} point group. Among 18 calculated wavenumbers, six are displayed in the figure. They (<1000 cm^{-1}) are not fit for the observed IR data. Thus, the tridentate adsorption is not relevant to the present IR assignment. When the NO• radical is captured to form the tridentate structure, NO desoprtion would be difficult. The adsorption energy is calculated to be 4.2 eV relative to the energies of $(MgO)_4$ and NO. In the IR experiment, the temperature has been increased to 470 K after the adsorption, and the main products of TDs in this temperature region were NO molecules based on the TPD measurements. Therefore, the NO species in the tridentate form would be retained (although not detected in the present IR study) and doped on the MgO surface under the temperature conditions.

Four types of adsorptions in Scheme 2 have been investigated by the use of cluster model calculations. Monodentate (1), asymmetric (2), and symmetric (3) bidentate adsorptions correlate reasonably with the IR results. IR observable frequencies arise basically from local MgO_2N and MgO_2N^+ species. The type 1 monodentate model has been converted to the type 2 asymmetric bidentate model through an electron loss (Scheme 3).

Examination of the isotope effect on frequencies shows that the $^{16}O^{14}N \rightarrow {}^{18}O^{15}N$ substitution of the adsorbate has generally lowered them. In addition, some bands have been split by this effect (Figure 1). The splitting has been suggested in the previous section to come from the coexisistance of $^{16}O^{15}N^{18}O$ and $^{16}O^{15}N^{16}O$ species. The splitting is examined in Figure 9. The figure exhibits three wavenumbers of the NO_2 moiety in a model MgO_2N and type 3 $(MgO)_4NO$ geometries. Those in two geometries have similar values. In species A′ of Figure 1, 1205 cm^{-1} of the $^{14}N^{16}O$ adsorbate has shifted to 1171 and 1162 cm^{-1} of the $^{15}N^{18}O$ one. The change of experimental values, 1205 → (1171, 1162) in Scheme 1 is similar to that of the experimental numbers, 1259 → (1236, 1224) in Figure 9. Also, the change, 1167 → (1134, 1118) in Scheme 1 is similar to that of theoretical numbers, 1219 → (1193, 1176) in Figure 9. The similarity of the splitting extent between measured wavenumbers (Scheme 1) and calculated ones (Figure 9) has been determined. Formation of the $^{16}O^{15}N^{16}O$ species as well as the $^{16}O^{15}N^{18}O$ one is likely, and the oxygen exchange should take place on the MgO surface after the $N^{18}O$ adsorption at RT. From the $^{16}O^{15}N^{16}O$ species, its fragment radical $^{16}O^{15}N$ may be evolved (Scheme 4). This evolution has been demonstrated by the TPD spectra in the temperature region of 350−500 K and the disappearance of the IR absorption below 470 K (Figure 2). Thus, the isotope

effect on the present calculated wavenumbers explains the splitting of the type 3 IR bands and supports the oxygen exchange in the NO_2 species.

This study has adopted the B3-LYP/6-31G* computational method. The inclusion of diffuse polarization functions, i.e., B3-LYP/6-31+G*, decreases the wavenumbers slightly (~10 cm^{-1}).[13] Besides geometries in Figures 4−8, many other models have been examined to check the agreement between the FT-IR and calculated models. The present IR data and various computational results are displayed in Figure 10.

V. Concluding Remarks

This work has dealt with FT-IR spectroscopic investigations and ab initio calculations of the NO adsorption on the MgO surface. Isotope effect and temperature dependence of the IR spectra have produced three types of adsorbed species. Those types have been ascribed to three kinds of the adsorption: type 1, monodentate; type 2, asymmetric bidentate; type 3, symmetric bidentate. The shift of three types, (1) → (2) → (3), would correspond to the change of molecular characters of the adsorbate, NO → O···N−O → O−N−O. A stronger adsorption than these three leads to the type 4 tridentate. This model gives, however, <1000 cm^{-1} wavenumbers owing to three weakened N−O bonds and is not fit for the present IR data. An oxygen exchange, $^{16}O^{15}N^{18}O \rightarrow {}^{16}O^{15}N^{16}O$, has been suggested by the FT-IR isotope effect and has been supported by DFT calculations. A plausible mechanism of the four adsorption patterns on a typical MgO (001) surface with a step may be deduced from the present IR calculation combined study and is shown in Scheme 5. An on-top NO adsorption at a four-coordinated Mg_{4C} site on a ledge forms the type 1 monodentate. An NO adsorption at O_{4C} site with a nearby Mg_{4C} forms the type 2 asymmetric bidentate NO_2. An NO adsorption at the $O_{3C}-Mg_{4C}$ pair at the kink site may form the type 3 symmetric bidentate NO_2, when O_{3C} is left from the lattice site. At the particular site, e.g., a cation−anion vacancy pair site at a step, NO may be adsorbed and may be trapped at cation (N) and anion (O) sites, respectively, to form the type 4 "tridentate" NO_3-like species.

Supporting Information Available: Cartesian coordinates of geometries optimized by R(or U)UB3-LYP/6-31G* in Figures 3−8 and 10. This material is available free of charge via the Internet at http://pubs.acs.org.

References and Notes

(1) Srnak, T. Z.; Dumesic, J. A.; Clausen, B. S.; Törnovist, E.; Topsøe, N.-Y. *J. Catal.* **1992**, *135*, 246.
(2) Udovic, T. J.; Dumesic, J. A. *J. Catal.* **1984**, *89*, 314.
(3) Cerruti, L.; Modone, E.; Guglielminotti, E.; Borello, E. *J. Chem. Soc., Faraday Trans. 1* **1974**, *70*, 729.
(4) Yanagisawa, Y. *Appl. Surf. Sci.* **1995**, *89*, 251.
(5) Hehre, W. J.; Radom, L.; Schleyer, P. v. R.; Pople, J. A. *Ab initio Molecular Orbital Theory*; Wiley: New York, 1986; Chapter 6.3.
(6) Pople, J. A.; Schlegel, H. B.; Krishnan, R.; DeFrees, D. J.; Binkley, J. S.; Frisch, M. J.; Whiteside, R. A.; Hout R. F.; Hehre W. J. *Int. J. Quantum Chem., Quantum Chem. Symp.* **1981**, *15*, 269.
(7) Frisch, M. J.; Trucks, G. W.; Schlegel, H. B.; Gill, P. M. W.; Johnson, B. G.; Robb, M. A.; Cheeseman, J. R.; Keith, T.; Petersson, G. A.; Montgomery, J. A.; Raghavachari, K.; Al-Laham, M. A.; Zakrzewski, V. G.; Ortiz, J. V.; Foresman, J. B.; Cioslowski, J.; Stefanov, B. B.; Nanayakkara, A.; Challacombe, M.; Peng, C. Y.: Ayala, P. Y.: Chen, W.: Wong, M. W.; Andres, J. L.: Replogle, E. S.; Gomperts, R.; Martin, R. L.; Fox, D. J.; Binkley, J. S.; Defrees, D. J.; Baker, J.; Stewart, J. P.; Head-Gordon, M.; Gonzalez, C.; Pople, J. A. *Gaussian 94*, revision D.4; Gaussian, Inc.: Pittsburgh, PA, 1995.
(8) (a) Becke, A. D. *Phys. Rev.* **1988**, *A38*, 3098. (b) Becke, A. D. *J. Chem. Phys.* **1993**, *98*, 5648.
(9) Foresman, J. B.; Frisch, Æ.; *Exploring Chemistry with Electronic Structure Methods*, 2nd ed.; Gaussian, Inc.: Pittsburgh, PA, 1995−1996; Chapter 7.
(10) Clark, T.; Chandrasekhar, J.; Spitznagel, G. W.; Schleyer, P. v. R. *J. Comput. Chem.* **1983**, *4*, 294.
(11) Busca, G.; Lorenzelli, V. J. *Catalysis* **1981**, *72*, 303.
(12) Snis, A.; Panas, I. *Surf. Sci.* **1998**, *412/413*, 477.
(13) The wavenumbers of NO_2^-, $(MgO)_4NO^-$, $(MgO)NO^-$, and NO_3^- calculated by B3-LYP/6-31G* (unscaled) are compared with those by B3-LYP/6-31+G*, below. As far as three wavenumbes of the NO_2 moiety are concerned, the former method gives slightly larger ones (at most 10 cm^{-1}) than does the latter.

Comparison of Calculated Wavenumbers (cm^{-1})

model species	B3-LYP/6-31G*	B3-LYP/6-31+G*
NO_2^-	792	788
	1341	1317
	1378	1342
$(MgO)_4NO^-$	874	870
	1314	1302
	1362	1359
$(MgO)NO^-$	843	839
	1309	1290
	1350	1257
NO_3^-	706	697
	706	697
	838	827
	1077	1070
	1469	1401
	1470	1402